Mathematical Biosciences 220 (2009) 24–33

Contents lists available at ScienceDirect

Mathematical Biosciences

journal homepage: www.elsevier.com/locate/mbs

Epidemic patch models applied to pandemic influenza: Contact matrix, stochasticity, robustness of predictions

Antonella Lunelli [a,*], Andrea Pugliese [a], Caterina Rizzo [b]

[a] Department of Mathematics, University of Trento, via Sommarive 14, 38100 Povo (TN), Italy
[b] National Center for Epidemiology, Surveillance and Health Promotion, Istituto Superiore di Sanità, Italy

ARTICLE INFO

Article history:
Received 10 October 2008
Received in revised form 17 March 2009
Accepted 31 March 2009
Available online 14 April 2009

Keywords:
Infectious disease modelling
Pandemic influenza
Model design and parameterisation

ABSTRACT

Due to the recent emergence of H5N1 virus, the modelling of pandemic influenza has become a relevant issue. Here we present an SEIR model formulated to simulate a possible outbreak in Italy, analysing its structure and, more generally, the effect of including specific details into a model. These details regard population heterogeneities, such as age and spatial distribution, as well as stochasticity, that regulates the epidemic dynamics when the number of infectives is low. We discuss and motivate the specific modelling choices made when building the model and investigate how the model details influence the predicted dynamics. Our analysis may help in deciding which elements of complexity are worth including in the design of a deterministic model for pandemic influenza, in a balance between, on the one hand, keeping the model computationally efficient and the number of parameters low and, on the other hand, maintaining the necessary realistic features.

1. Introduction

In 1997, the emergence of the highly virulent A/H5N1 avian influenza strain [1] has raised concern over the risk of a future influenza pandemic [2]. The virus has proven its ability to pass directly from birds to humans [3] and could potentially acquire the capacity for efficient person-to-person transmission. Therefore it is considered to be the leading contender as the source of the next human influenza pandemic [4,5]. Nowadays, the increasing mobility of the population at a global level and the speed of means of transport would make the control of the spread of infection particularly problematic. For these reasons, countries have been urged to strengthen their preparedness plans [6], following the 2005 WHO recommendations [7].

A range of measures have been suggested in order to contain a possible pandemic, including those that involve personal actions (such as hand-washing and mask wearing), non-pharmaceutical interventions (like international air travel restriction, social distancing measures and quarantine [8]), and pharmaceutical interventions (like antiviral drugs and vaccines [4]). Application of public health measures will reduce the number of people who are infected, need medical care and die during an epidemic, thus lessening the impact of mass absenteeism on key functions (e.g. delivering health care, food supplies, fuel distribution, etc.). Several countries are therefore planning a wise use of available resources, using mathematical models to obtain quantitative estimates of the likely pattern and speed of propagation of a pandemic and of the possible impact of different interventions [9–14].

Very detailed individual based models have been developed [12,13,15–19]. These models simulate the stochastic spread of influenza in populations of persons interacting in known contact groups, according to real sociodemographic data. They represent a typical heterogeneous community and allow for detailed predictions, but they require many data, often not available.

On the other hand, classical deterministic compartmental models have the main advantage of simplicity. They involve relatively few parameters and have been considered as an initial step, before more complicated models are invoked [20,21]. When little is known about the disease and parameter values can only be guessed, they represent an effective tool that can easily be adapted to different, still unknown, settings. These models have been suggested for the analysis in specific regions [20,22], but have also been extended to predict the geographic spread of the disease [23–26]. In this case the environment is often divided into discrete regions, called patches, with the individuals moving through different patches and thus spreading the infection.

Here we analyse the SEIR model used to simulate the spread of pandemic influenza in Italy [27]. The model includes an age-and-space contact matrix, which has been built from available census data. We give the details of the estimation procedure and, through the comparison with a population survey-based contact matrix, we show that our procedure supplies a reliable matrix of contacts. We describe the model in all its components, discussing the specific

* Corresponding author. Tel.: +39 0461 883983; fax: +39 0461 881624.
E-mail address: alunelli@science.unitn.it (A. Lunelli).

0025-5564/$ - see front matter © 2009 Elsevier Inc. All rights reserved.
doi:10.1016/j.mbs.2009.03.008

modelling choices and presenting a systematic analysis of the influence of each component on the predicted epidemic curves. Our study provides a first assessment of the relevance of including precise details when modelling an epidemic with compartmental models and may help in deciding which elements of complexity are worth including in the design of a model. Our analysis may thus help to balance between the necessity of keeping the number of parameters low and the complexity of the model limited, and the necessity of having a realistic model, able to yield reliable simulations of epidemic scenarios. Finally, we show how we have organised the simulations and calibrated the model to simulate possible pandemic scenarios and how the parameter choices influence the evaluation of the effectiveness of control strategies.

2. The model

The model is structured as an SEIR model. The population is divided into four classes according to the disease state: susceptible (S), exposed (E), infectious (I) and removed (R) individuals. People who become infected enter the latent period during which they do not show symptoms and cannot spread the infection. This is followed by the infectious period that ends when the individuals recover or die. For simplicity, we do not distinguish between symptomatic and asymptomatic infectives, who, as often assumed, may differ in their infectiousness [12,19].

Epidemic dynamics are influenced by population heterogeneities (e.g. influenza incidence may vary considerably with age [28]) and individual contacts are definitely not homogeneous. Moreover, control strategies are often designed differently for different age groups [29]. In order to include these aspects into the model, the population has been divided in groups.

We have defined six age classes for age-specific control measures: infants 0–2 years of age, children 3–14 years of age, teenagers 15–18 years of age, young adults 19–39 years of age, adults 40–64 years of age and elderly aged 65 or more. Furthermore, each age class has been divided in two subclasses, depending on activity level: a part of the population will be more active and will have a higher number of social contacts, while another part will spend more time at home and thus have fewer social contacts. Although such a distinction is clearly simplistic, it reflects existing population heterogeneities, and makes simulated epidemic curves fit better to simulated data from individual-based models, as those proposed by Ciofi degli Atti et al. [19]. Individuals are then located in subgroups corresponding to the Italian geographical regions.

Thus, each population group is identified by two indexes: $i = 1, \ldots, m$, representing age and/or activity intensity, and $p = 1, \ldots, s$, denoting the spatial region where the individual lives. Considering two activity groups for each age-class and 20 geographical patches gives $m = 12$ and $s = 20$.

We will use the variables S_i^p, E_i^p, I_i^p and R_i^p, representing the number of susceptibles, exposed, infectives and removed of class i in region p. The population size N_j^p of each class of each region is supposed to be constant, which seems a reasonable hypothesis due to the short epidemic course of influenza.

Finally, the model is described by the following system of differential equations:

$$\begin{cases} \frac{dS_i^p}{dt} = -S_i^p \sum_{j,q} \beta_{ij}^{pq} \frac{I_j^q}{N_j^q} \\ \frac{dE_i^p}{dt} = S_i^p \sum_{j,q} \beta_{ij}^{pq} \frac{I_j^q}{N_j^q} - \nu E_i^p \\ \frac{dI_i^p}{dt} = \nu E_i^p - \gamma I_i^p \\ \frac{dR_i^p}{dt} = \gamma I_i^p \quad i,j = 1,\ldots,12 \\ \qquad\qquad p,q = 1,\ldots,20 \end{cases} \tag{1}$$

where $1/\nu$ and $1/\gamma$ represent, respectively, the mean length of the latency and the infectivity periods. In all simulations we fixed these values to 1 [30] and 4 [15,31,32] days, respectively.

The transmission rate β_{ij}^{pq} represents the average number of individuals of class j and region q with whom a susceptible of class i and region p makes a contact sufficient to result in transmission in the unit time. A fraction I_j^q/N_j^q of these individuals will be infectious and so the susceptible will be infected. To a large extent, the behaviour of the model is determined by the $(s \cdot m) \times (s \cdot m)$ (in our case 240×240) contact matrix. Obtaining a reliable estimate of 240^2 parameters would require many unavailable data, and also performing a sensitivity analysis on all of them is unfeasible. Therefore, we have made a priori specific assumptions on the structure of the matrix, used independent information to approximate the value of some parameters, and finally left a couple of free parameters, on which it was possible to perform a sensible sensitivity analysis. Details on how we built the contact matrix are given in the next subsection.

2.1. The structure of the contact matrix

The contact matrix β_{ij}^{pq} has been structured considering separately contacts among regions and among activity/age groups within a region.

Coupling between different regions has been implemented distinguishing between long- and short-distance travelling. Long-distance travelling has been modelled through a national air-traffic matrix F, whose element F^{pq} is defined as the mean weekly number of flights from region p to region q. Air transportation data have been obtained from the web sites of Italian airports and refer to the winter season 2005–2006. Short-distance travelling is represented by a symmetric contact matrix T, whose pq entry is 1 if daily travelling between regions p and q is possible and 0 otherwise. Therefore all patches are directly or indirectly connected and travelling individuals can spread the infection from region to region. Only active adults are allowed to travel from one region to another. In other words, we assumed that movements of less active people, children, teenagers and elderly are negligible, so that individuals of different regions may interact only if they are active adults.

Finally the contact matrix has been defined as follows:

$$\beta_{ij}^{pq} = \begin{cases} \beta_{ij} & \text{if } p = q \\ 0 & \text{if } p \neq q \text{ and } i \text{ or } j \\ & \text{are not active adults} \\ \beta_{ij} M^{pq} & \text{if } p \neq q \text{ and } i,\ j \text{ are both} \\ & \text{active adults} \end{cases} \tag{2}$$

where

$$M^{pq} = \varepsilon \left(\delta F^{pq} + \frac{T^{pq} N^q}{\sum_r T^{pr} N^r} \right) \tag{3}$$

represents the proportion of effective contacts between adults of different regions compared to adults of the same region.

Note that the formula implies that people travel to the neighbouring regions proportionately to their population sizes, which is an usual assumption [19] lacking precise data. F and T are the transportation matrices defined before, while ε and δ represent the weights of short and long distance travels, respectively. ε has been calibrated according to the Italian National Statistical Office (ISTAT) data, according to which approximately 2% of people travel daily to neighbouring regions. No data are available on long distance travelling between regions, hence δ will be used as a free parameter that measures the importance of long distance vs. short distance travel.

Table 1
Average number of contacts between age groups in households (top table) and in schools/workplaces (at the bottom) estimated as described in the main text. The population is divided in six age classes: infants 0–2 years of age, children 3–14 years of age, teenagers 15–18 years of age, young adults 19–39 years of age, adults 40–64 years of age and elderly aged 65 or more.

c^f_{ij}	0–2	3–14	15–18	19–39	40–64	$\geqslant 65$
0–2	0.09	0.7	0.004	1.55	0.3	0
3–14	0.13	0.67	0.14	1	1	0.04
15–18	0.002	0.34	0.12	0.3	1.55	0.06
19–39	0.15	0.5	0.05	0.54	0.91	0.01
40–64	0.03	0.24	0.19	0.43	0.59	0.17
$\geqslant 65$	0	0.03	0.01	0.01	0.3	0.37
c^s_{ij}	0–2	3–14	15–18	19–39	40–64	$\geqslant 65$
0–2	1.9	0	0	0.6	0.19	0.8
3–14	0	19	0	1.43	1.43	0
15–18	0	0	15.8	1.37	1.37	0
19–39	0	0	0	2.83	1.83	0
40–64	0	0	0	1.59	1.59	0
$\geqslant 65$	0.12	0	0	0	0	0

As for the within region contacts between age/activity classes, we have followed the basic idea developed in individual based models [13,15–17,30]: influenza transmission may occur in consequence of a contact with an infectious at home, at school/work or because of an occasional contact within the community. We have further assumed that these three components of the risk of infection have the same magnitude:

$$\beta_{ij} = \vartheta^f c^f_{ij} + \vartheta^s c^s_{ij} + \vartheta^o c^o_{ij} \tag{4}$$

with

$$\sum_j \vartheta^f c^f_{ij} \approx \sum_j \vartheta^s c^s_{ij} \approx \sum_j \vartheta^o c^o_{ij} \tag{5}$$

where $c^f_{ij}, c^s_{ij}, c^o_{ij}$ represent the average number of contacts that an individual of class i has with an individual of class j, respectively, at home, at school/work, or in other circumstances and ϑ^f, ϑ^s, ϑ^o represent the probabilities that these contacts result in successful transmission of the infection.

To estimate the average number of contacts c^f_{ij} and c^s_{ij} we have used the 2001 Italian census data[1] on the composition of households, school attendance and employment condition. Namely, in order to evaluate c^f_{ij} we have estimated from the data the mean number of family members that an individual in class i has in class j; since data in this exact form are not available, our estimate uses a guess on the age difference between siblings, but the resulting matrix is rather robust to this choice. To estimate c^s_{ij} we have used the data on school attendance and employment rate in the various classes; school contact rates are computed assuming an average of 20 schoolmates of the same age group (the number is reduced to 10 for daycare centres) and also some fringe contacts between students and teachers and between grandparents and grandchildren who do not attend daycare. Finally, work contact rates are distributed between age classes in relation to their contribution to the work–force; given the usual estimate of a lower force of infection in older age classes for air-borne transmitted childhood diseases such as measles or chickenpox [33,34], their total strength is taken as one-sixth of the weight of school contacts. The resulting matrices are given in Table 1.

As for contacts within the community, we have assumed that the probability $\vartheta^o c^o_{ij}$ of getting the infection from an individual of class j occasionally met is proportional to the size N_j of class j, that is $\vartheta^o c^o_{ij} \approx K N_j$, where K is the constant of proportionality that needs to be estimated.

[1] Available at: www.istat.it

Using (5), we have the following relations:

$$\vartheta^s \approx \vartheta^f \frac{\overline{\sum_j c^f_{ij}}}{\overline{\sum_j c^s_{ij}}} \quad K \approx \vartheta^f \frac{\overline{\sum_j c^f_{ij}}}{\overline{\sum_j N_j}}, \qquad i,j = 1,\dots,m \tag{6}$$

where the bar represents the average value computed over all classes. These relations, together with the estimates of c^f_{ij}, c^s_{ij} and the data N_j, allow for the definition of the three components of β_{ij} once we have fixed the free parameter ϑ^f.

We assume that the contact rates for the less active groups have the same structure but are suitably reduced. Namely, we have a reduction factor ρ if the contact is between a more active and a less active individual and a reduction factor $\rho/2$ if the interaction is between two individuals with few social contacts, i.e.

$$\beta_{i+\frac{m}{2},j} = \rho\beta_{i,j} \quad \beta_{i,j+\frac{m}{2}} = \rho\beta_{i,j} \quad \beta_{i+\frac{m}{2},j+\frac{m}{2}} = \frac{\rho}{2}\beta_{i,j}, \quad i,j = 1\dots\frac{m}{2} \tag{7}$$

(classes 1 to $\frac{m}{2}$ represent more active individuals, while classes $\frac{m}{2}+1$ to m are the less active).

In summary, the calibration of the within region contacts depends on two parameters. One (ϑ^f) is related to virus transmissibility and the other (ρ) reflects population heterogeneity: if ρ is close to 1 there is little difference between the transmission rates of more and less active individuals and so the level of heterogeneity in the population is low, while, if ρ is close to 0, heterogeneity is much higher and there is a sensible difference in virus transmission between individuals with different social behaviour.

2.1.1. Validation of the contact matrix

As explained above, our matrix of contacts has been estimated using available data from the 2001 census, integrated with a priori assumptions that appeared reasonable. To verify the reliability of our estimation procedure we have compared our matrix with the matrix obtained from the results of a population-based survey on contact patterns recently published [35]. The survey provides the first quantitative information on contact patterns. We have used the data in the form of a matrix, deriving the average number c_{ij} of contacts that a person in age class i has daily with individuals in class j. As done with our contact matrix, we have calibrated these numbers introducing a probability ϑ of being infected after a contact with an infectious (corresponding to $\vartheta^f, \vartheta^s, \vartheta^o$, of (4)) and a reduction coefficient ρ (see (7)) that reduces the number of contacts with less active people.

2.2. Organisation of simulations

Data from the Italian National Statistical Office (ISTAT) on spatial and age distributions have been used to define the demographic structure of the population and to distribute the individuals in age classes and regions. In each age class individuals have been classified as more or less active, assuming that infants, children and elderly tend to have few social contacts, while teenagers and adults are more active. The subdivision (see Table 2) is

Table 2
Proportion of more and less active individuals in each age class.

Age class	More active (%)	Less active (%)
0–2	25	75
3–14	35	65
15–18	50	50
19–39	50	50
40–64	50	50
65 and older	25	75

somehow arbitrary but its effect on the overall heterogeneity is regulated by the parameter ρ, described above.

As an initial condition for the simulations we assume that the population is completely susceptible to the wave of infection. The epidemic is initialised introducing 5 infected individuals in Italy. The infected are all young adults and, when spatial structure is included, they are placed in the Lazio region, where the intercontinental airport of Rome is located. Our choice is motivated by the likely assumption that the virus would initially come from abroad. We did not find any substantial difference in the simulated epidemics locating the initially infected individuals in other regions with international airports.

As for the values of the free parameters δ, ϑ^f and ρ, a guideline in the choice is the value of the basic reproductive ratio R_0, the average number of secondary cases produced by a single typical infectious individual in a completely susceptible population. R_0 is defined, using the method of Diekmann and Heesterbeek, as the dominant eigenvalue of the next generation matrix [36], that we have computed through the contact matrix β_{ij}^{pq} defined by (2).

Another indicator of an epidemic is the overall attack rate, i.e. the fraction of the population eventually infected. In a homogeneous population this is completely determined by R_0 [36], while, in a heterogeneous population, to a fixed value of R_0 may correspond different attack rates. In fact, while the value of R_0 depends mainly on the contact rates of the more active classes [37], the level of heterogeneity determines the attack rate. With high heterogeneity less active people have very few contacts and will be unlikely to get infected and spread the infection, thus the global attack rate will be low. On the other hand, with low heterogeneity, less active people have contact rates similar to those of more active people and will be more likely to get infected and infect others, thus incrementing the attack rate. Therefore, fixed R_0, the more heterogeneous the population, the lower will be the global attack rate.

This is shown in Fig. 1, using ϑ^f and ρ as parameters. The figure displays the contour plots for R_0 and the attack rate AR as a function of the two parameters, showing that the attack rate increases rapidly with ρ (that is decreasing heterogeneity), while R_0 depends more significantly on ϑ^f. The figure has been obtained fixing $\varepsilon = 0$, that is ignoring the spatial component; very similar curves are obtained for $\varepsilon = 0.02$ (the reference value) and any fixed value of $\varepsilon \neq 0$.

Estimates of R_0 for past pandemics vary widely, ranging from 1.5 to 3.9 [12,21,38–42]. We have generated the baseline epidemic choosing $R_0 = 1.8$, that is considered a realistic estimate for the basic reproductive ratio of a possible pandemic [25,12]. Then we have considered a milder and a more severe scenario, characterised by $R_0 = 1.6$ and 2.0, respectively.

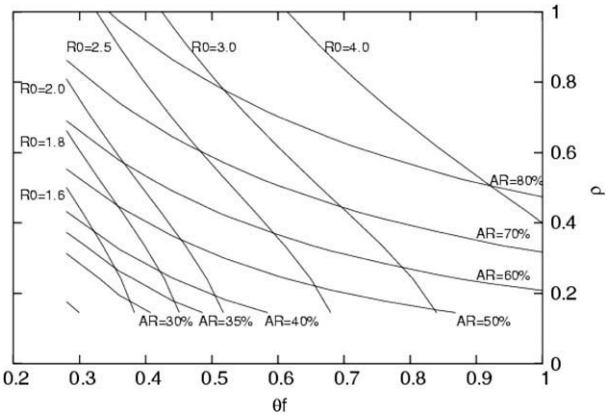

Fig. 1. Contour plots of the reproduction ratio R_0 and the global attack rate AR, as a function of the parameters ϑ^f and ρ with $\varepsilon = 0$.

The clinical reported attack rate for past pandemics is about 31–33% [16,21], but much higher estimates have been obtained for the serological attack rates [21]. We have considered an attack rate of 35% (corresponding to high heterogeneity) in the baseline scenario, and then we have increased it up to 50% (corresponding to low heterogeneity).

The free parameter δ has been chosen making different hypothesis on long-distance travelling. We have assumed that short distance movements count as much as, twice as much (baseline scenario) or four times as much as long distance travelling. This gives, respectively, $\delta = 3.4 \times 10^{-3}, \delta = 1.7 \times 10^{-3}$ and $\delta = 8.5 \times 10^{-4}$.

In order to obtain the given values of R_0 and the attack rate, we have calibrated the parameters ϑ^f and ρ, realising contour plots similar to those shown in Fig. 1, but for the correct values of ε and δ. In the baseline scenario, with $\delta = 1.7 \times 10^{-3}$, $R_0 = 1.8$ and $AR = 35\%$, we have set $\vartheta^f = 0.445$ and $\rho = 0.17$, the point where the contours $R_0 = 1.8$ and $AR = 35\%$ intersect.

2.3. The stochastic component

As well known, deterministic compartmental models like (1) are not appropriate to correctly describe the dynamics of an epidemic, especially during the initial and final phases, when a small number of individuals is infected and stochastic factors play a major role. Moreover, in our model we have a large number of compartments that may not be all directly connected, so that even when the overall number of infective individuals is large, the expected number of infectives may be very low in several compartments. It is thus conceivable that stochastic factors have a relevant influence not only in the very initial and final phases.

To adequately model such phenomena we have introduced a stochastic component that regulates the spread of the infection when the number of infectives is sufficiently low. Namely, at each time step of the differential equation solver, if the total number of exposed and infected in a region/class (E_i^p or I_i^p) predicted by Model (1) was below a threshold value (we chose a value of 10), it was replaced by a Poisson variable with that mean. This is a simplified and computationally inexpensive way to include stochasticity into the model, that has been successfully considered in epidemic modelling applications [43–47].

To investigate the reliability of this approximation we have compared some of the results with those obtained with a full stochastic model, simulated as a continuous-time Markov chain with the rates specified consistently with (1), using the Gillespie algorithm [48].

3. Numerical simulations and results

Our baseline scenario has been simulated taking $R_0 = 1.8$, $AR = 35\%$ and $\delta = 1.7 \times 10^{-3}$ and including the stochastic component, implemented using the Poisson approximation described above. This implies that all simulations are different, with some of them dying out spontaneously after a handful of cases (the distinction between these and substantial epidemics is always quite clear-cut). Simulations that give rise to an epidemic are rather different from each other, mainly in the length of the initial phase, before a considerable number of cases builds up (see left panel of Fig. 2). The epidemic peak is reached, on average, after 16.6 weeks, with a 90% confidence interval given by (15.1–18.7). To define a "typical epidemic curve", we superimposed the peaks of all epidemic curves (for the simulations giving rise to an epidemic) and computed the average incidence at each time relative to the peak time. The resulting curve has then been shifted to locate

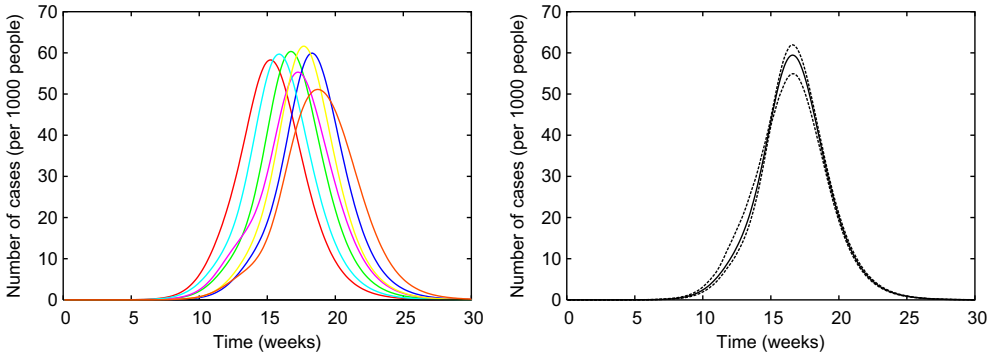

Fig. 2. Epidemic curves obtained simulating an uncontrolled influenza pandemic in Italy. The figure shows some of the simulations obtained implementing the Poisson stochastic approximation (on the left) and (on the right) the average epidemic curve (solid line) with 90% confidence curves (dashed lines) calculated superimposing all the curves, as described in the text.

the peak at the average peak time, to produce the curve defined as "the typical simulation". Analogously we have calculated 90% confidence curves, computing at each relative time 90% confidence intervals for the predicted incidence (see right panel of Fig. 2).

3.1. Spatial structure

We have analysed the importance of including a spatial structure in the model running the model with and without the spatial structure, for the scenario with $R_0 = 1.8$ and $AR = 35\%$. In the model without spatial structure we have divided the Italian population in 12 age/activity classes and used the matrix β described through (4) as contact matrix; in the spatial model we have used (2) as contact matrix, including the movement matrix (3) that depends on the two parameters, ε and δ. ε was fixed at 0.02, while δ (representing the relative weight of long vs. short distance travelling) has been varied as discussed above.

Fig. 3 shows the results obtained running, for each scenario, 200 stochastic simulations with the Poisson stochastic component described above. This figure shows some of the predicted curves (left panel) and "the typical simulation" (right panel) with and without spatial structure, for different values of δ.

Even if the cumulative incidence and the duration of the epidemic are approximatively the same with and without spatial structure, we can see how, if no spatial structure is included, the epidemic is much quicker and reaches its peak 3–4 weeks in advance with a somewhat higher incidence during the peak week. On the other hand, results do not seem to be significantly related to the relative weight of long distance travelling. Single simulations are overlapping and the typical epidemic curve is only slightly delayed when long distance movements are weighted less, as one can expect.

3.2. Stochastic component

In order to assess the role of stochasticity, we have compared a deterministic, a full stochastic model and our stochastic correction of the deterministic model, considering the baseline scenario ($R_0 = 1.8,\ AR = 35\%$ and $\delta = 1.7 \times 10^{-3}$).

Fig. 4 shows the results obtained, displaying some of the simulations run and the typical epidemic curves. We can see that, on average, there is only a small difference between the three models. The typical stochastic curves are very similar to each other and are only slightly different from the deterministic one: the epidemic peak is slightly delayed (16.1, 16.4 and 16.6 weeks for the deterministic, full stochastic and Poisson model, respectively) and slightly lower (63.5, 59.6 and 59.5 cases per 1000 people) than in the deterministic model. The global attack rate is the same in the three cases (35%).

Instead, looking at the single stochastic simulations, we observe a considerable variability in the length of the initial phase, before the exponential growth of the epidemic. This variability represents the main difference between stochastic and deterministic dynamics.

A summary of the results obtained with the two stochastic models is given in Table 3. The results are fairly similar, at least for the simulations that give rise to an epidemic. In both cases the epidemic peak occurs during the 16th week with a maximum incidence of approximately 60 cases per 1000 individuals. The variability in the initial phase, defined as the time needed to have 5

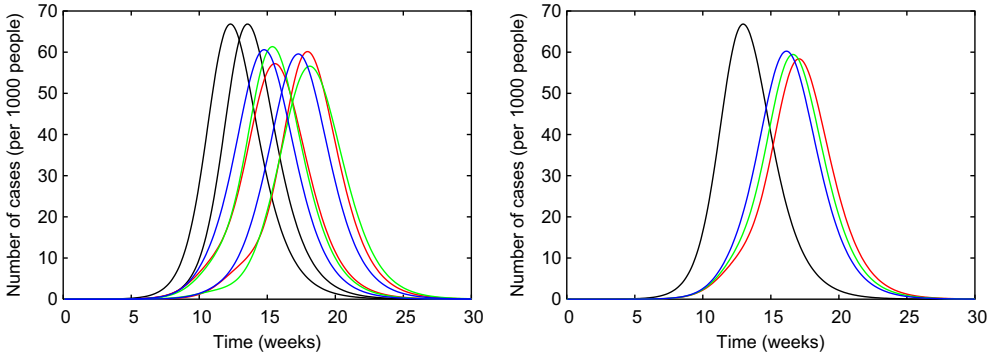

Fig. 3. The effect of the inclusion of the spatial structure on the predicted dynamics of influenza in Italy. The graphs show some simulations (on the left) and the average epidemic curve (on the right) obtained with the model without spatial structure (black lines) and with a spatial structure based on Italian regions, for different weights of long distance travels ($\delta = 8.5 \times 10^{-4}$ red line, $\delta = 1.7 \times 10^{-3}$ green line, $\delta = 3.4 \times 10^{-3}$ blue line).

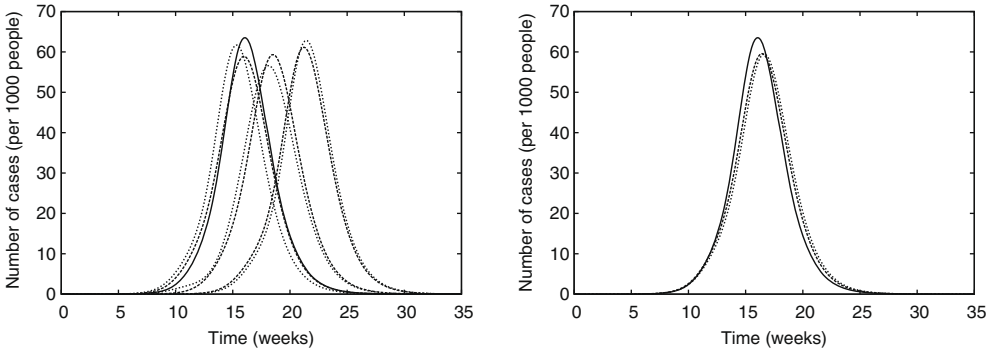

Fig. 4. Comparison between the epidemic curves predicted by a deterministic and a stochastic model. The figure shows three simulations (on the left) and the average epidemic curve (on the right) obtained with a deterministic model (solid line), a full stochastic model (dashed line) and our model (dotted line), where stochasticity is included through the Poisson approximation. The three simulations shown have been chosen so as to match the first part of the epidemic curves.

Table 3
Comparison of the two stochastic models. Numbers in parentheses indicate the empirical 90% confidence interval.

	Markov process	Poisson approximation
Time to infection peak	16.4 (15.3–18.3)	16.6 (15.1–18.7)
Prevalence at peak	59.6 (55.5–62.0)	59.5 (54.9–62.0)
Time to 5‰ prevalence	10.9 (9.7–12.7)	11.0 (9.6–13.2)
Frequency of early extinctions	11%	43.5%
CPU time for 10 simulations with large epidemic	2500 s	16 s

infected per 1000 individuals, is also very similar with 90% confidence intervals of 9.6–13.2 vs. 9.7–12.7 with the two models. On the other hand, there is a big difference in the probability of spontaneous extinction: 11% with the full stochastic model (Markov process) and 43.5% with the Poisson approximation, which clearly is an overestimation.

The time required to run the simulations is also very different for the two stochastic approaches: in our simulations, with about 57 million individuals, divided in 240 groups, the model with the Poisson approximation is much faster, requiring 16 vs. 2500 CPU-seconds (32 s vs. 54 min real time) on a Intel(R) Pentium(R) 4 CPU 2.40 GHz for 10 simulations giving rise to a large epidemic.

3.3. Validation of the contact matrix

To compare our matrix, defined using available data from census integrated with reasonable assumptions, with the contact matrix estimated through the results of the population survey conducted by Mossong et al. [35], we have set the values of the parameters in order to simulate our baseline scenario ($R_0 = 1.8$ and $AR \approx 35\%$) and we have compared the epidemic curves predicted by the model with the two contact matrices.

The two transmission matrices for the more active classes (classes 1–6) are shown in Fig. 5a and b. There are small differences between the two matrices, the most relevant being in the transmission rates between younger individuals (classes 1–3) and adults (classes 4 and 5), which have been slightly overestimated using census data. The structure of the survey-based matrix is more diagonal than our matrix, but, on the whole, the two transmission matrices are fairly similar.

The average epidemic curves, computed over 200 simulations run using the two matrices, are shown in Fig. 5c and are almost perfectly overlapping. The contact matrix estimated through the survey certainly reflects more precisely the contact patterns in the populations; nevertheless the results of our simulations seem to be robust to small variations in the transmission matrix.

3.4. Possible pandemic scenarios

As explained before, in the baseline scenario the model has been calibrated to have an R_0 equal to 1.8 and an attack rate around 35%. Nevertheless, since nobody can know in advance what the characteristics of a future pandemic will be, it is necessary to analyse other scenarios. The epidemic dynamics and intensity are regulated through the value of the free parameters ϑ_f and ρ, that parameterise virus transmissibility and population heterogeneity (we have seen that the free parameter δ does not influence significantly the dynamics). We have considered different combinations of the two parameters that give rise to several possible pandemic scenarios. In particular we have combined the parameters to obtain a basic reproductive ratio between 1.6 and 2.0 and an attack rate between 35% and 50% (see Fig. 1).

Fig. 6 shows the typical epidemic curves obtained for the different scenarios considered, where the typical simulation has been computed as before superimposing all the curves and calculating the average incidence at each time. Expected epidemic curves are widely different, according to the values of the parameters.

As shown in Fig. 6 the initial growth rate is basically controlled by the value of R_0. This has to be expected, since there is a one-to-one relation (though model-dependent) between the reproductive ratio R_0 and the growth rate in the exponential phase. Moreover, when R_0 is larger, the epidemic starts earlier, it reaches its peak earlier with a higher peak incidence, and then dies off faster (the typical bell shape is wider if R_0 is lower).

On the other hand, for the same value of R_0, a variety of epidemic curves are possible, varying in the height at the peak and in the total attack rate, showing that the overall dynamics of an epidemic cannot be summarised by the single parameter R_0.

4. The simulation of control strategies

We have simulated the implementation of different control measures, considering all the pandemic scenarios described above and making different assumptions on measures efficacy.

We have considered strategies composed of one or more of the three following interventions: (i) vaccination, (ii) antiviral prophylaxis and (iii) quarantine (i.e. social distancing measures, such as the closure of schools, public offices and places of aggregation).

We have modelled the use of a vaccine effective 4 or 5 months after the start of the epidemic (see [27] for details) and varied its efficacy between 50% and 70% [15]. According to the simulated vaccination policy the population is divided into four prioritised categories: (i) personnel of health services and other essential services, (ii) elderly aged 65 and older, (iii) children and teenagers from 2 to 18 years old and (iv) healthy adults. We assume to

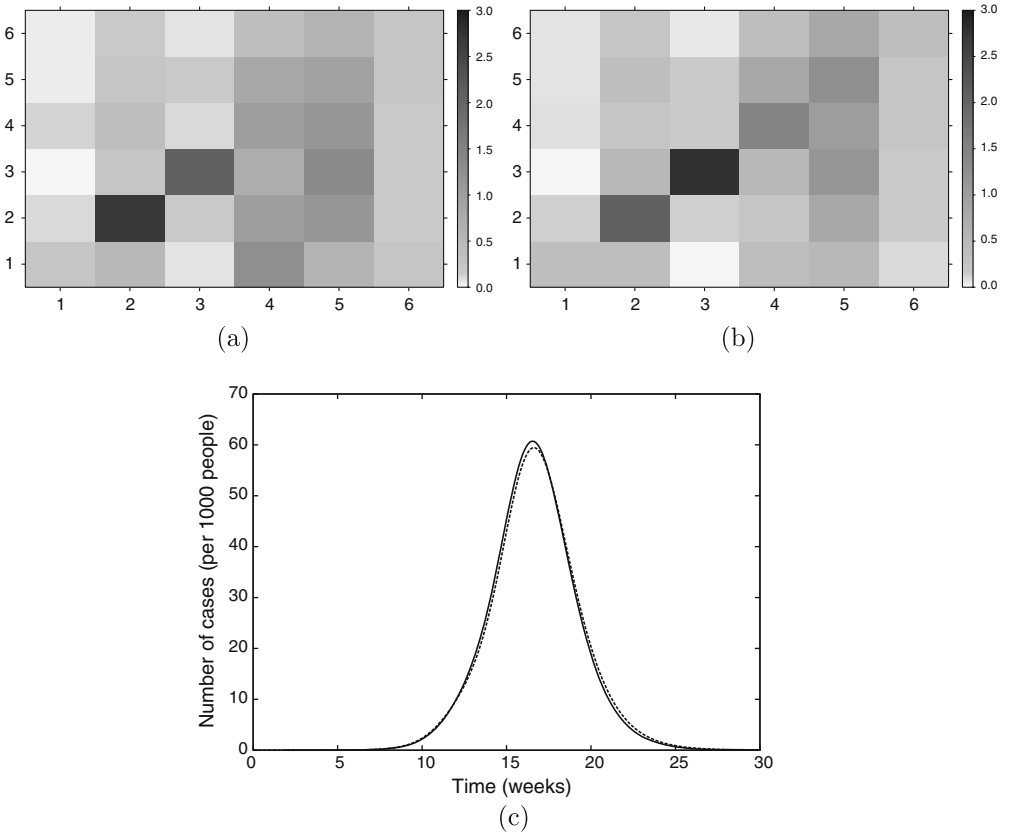

Fig. 5. A comparison between our transmission matrix (4) (a), estimated using available census data, and the transmission matrix estimated using the data from the population-based survey on contact patterns by Mossong et al. [35] (b). Cell ij corresponds to the transmission rate between class i and class j, for classes 1–6 (more active individuals). Darker colors correspond to higher transmission rates and numerical values (days^{-1}) are shown in the color-coded legend on the right side of each matrix. Transmission in less active classes has the same structure, but is reduced, as described in the main text. (c) The epidemic dynamics predicted by model (1) using transmission matrix (4) (dashed line) and the transmission matrix derived from the data published in [35] (solid line).

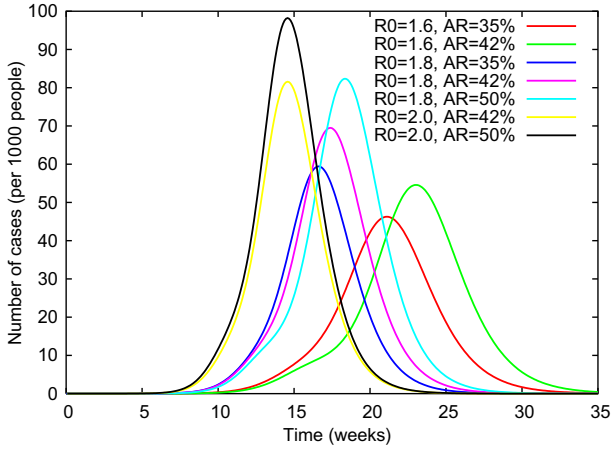

Fig. 6. Some scenarios of diffusion of an influenza pandemic in Italy. Epidemic curves obtained considering various combination of different hypothesis on virus transmissibility and population heterogeneity.

vaccinate all the categories starting from the first and that 2 weeks are necessary to deliver vaccine to each category.

Quarantine measures consist in the closure of schools, public offices and places of aggregation for 3, 4 and 8 weeks, respectively, starting 4 weeks after the first national cases. We assume that these measures would reduce the transmission rate within the community of 30%, 50% or 70%, while the effect of antiviral prophylaxis is a reduction of the transmission rate in households by 27%, 50% or 75%.

4.1. Results

The differences between expected epidemic curves in the absence of intervention clearly affect the effectiveness of control strategies.

A sample of results are shown in Fig. 7 and, as expected, the efficacy of control measures is much higher for low values of the reproductive ratio. For $R_0 = 1.6$ the attack rates can be reduced to values as low as 6%, while, for $R_0 = 2.0$, the global attack rate remains high (around 20%) also with the most successful strategy.

Interestingly, the effect of intervention seems to depend mostly on the value of R_0 and only marginally on the pandemic intensity, measured through the global attack rate. This fact can be explained observing Fig. 6 and noting that the start of the epidemic changes significantly with R_0, but only slightly when the attack rate increases and R_0 is kept constant. Since the effect of interventions strongly depends on timing [27], this determines the main differences observed in their effectiveness. The comparison between the case $R_0 = 1.8$, $AR = 50\%$ and the case $R_0 = 2.0$, $AR = 42\%$ is especially insightful. The two epidemic curves reach a similar peak, but differ in timing (the one with $R_0 = 2.0$ starts and reaches the peak earlier) and also in the overall attack rate. Assuming that an intervention strategy can be introduced at week 16, it is clear that it would be much more effective when $R_0 = 1.8$ and $AR = 50\%$ because, in the other case, the epidemic would already be in the

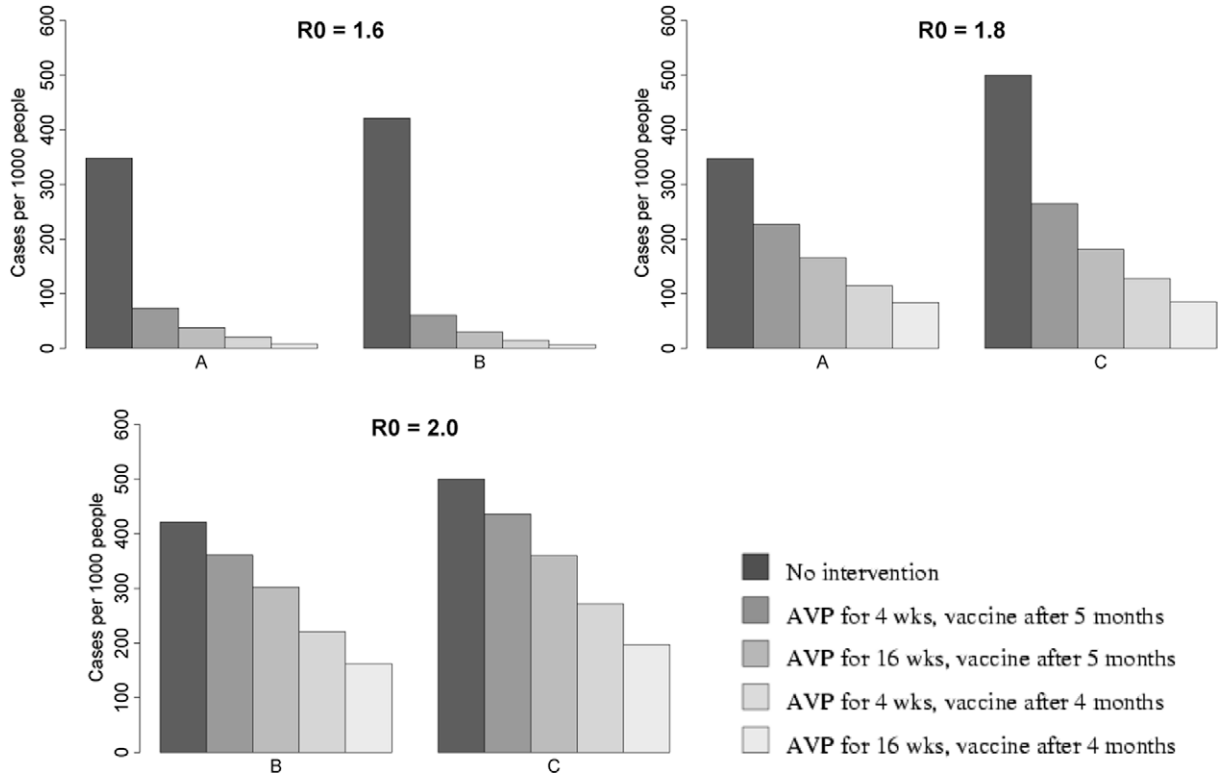

Fig. 7. Total attack rates for each combination of R_0 and *AR* without control and with a selected sample of control measures. Control measures consist in social distancing (with 50% efficacy) as described in the text, plus AVP (27% efficacy) and vaccination (70% efficacy) as indicated in the legend. A = high heterogeneity, corresponding to an attack rate around 35% without intervention, B = medium heterogeneity, corresponding to an attack rate around 42% without intervention, C = low heterogeneity, corresponding to an attack rate around 50% without intervention.

declining phase. So, even if the epidemic with $R_0 = 1.8$ is more intense ($AR = 50\%$ vs. 42%), it could be contained more successfully (compare in Fig. 7 the C panel with $R_0 = 1.8$ to the B panel with $R_0 = 2.0$).

Another aspect that influences the evaluation of intervention strategies is the assumed efficacy of the measures. Fig. 8a and b shows the effect of varying the efficacy of quarantine and antiviral prophylaxis; similar results have been obtained investigating the variability of vaccination efficacy [27]. As expected, a higher efficacy of the strategies increases the effectiveness of the intervention. Interestingly, when the efficacy of antiviral prophylaxis or quarantine is high the predicted epidemic has a longer tail, so that, even if the incidence during the peak weak is much lower, the reduction in the global attack rate is not as large.

The global attack rates for various intervention scenarios and different levels of strategies efficacy are presented in Fig. 8c. Vaccination plays a key role in pandemic containment (the combination of quarantine and antiviral prophylaxis is completely unsuccessful in reducing the attack rate, since they are simulated only as temporary measures) but it needs to be combined with other measures to be effective. Differences in the efficacy of single measures sometimes alter the ranking of the different combinations of measures, but under all assumptions the combination of all measures is the most effective way to contain a pandemic.

5. Discussion

In our work we have discussed the details included in an SEIR model built to simulate an influenza pandemic in Italy, investigating their importance and their influence on the simulated epidemic curves.

The population has been structured according to the age and spatial distribution of the individuals and a contact matrix has been derived from census data. Although the matrix could be improved if more detailed data were available, the results have proven to be robust to small variations in the transmission coefficients and encouragingly similar to those obtained with a contact matrix estimated from the survey-based contact patterns recently published by Mossong et al. [35]. Survey data are available for several European countries [35] but, for other countries not included in the survey or in other situations, a contact matrix could be obtained from census data, using the procedure described in this work. The simulated epidemic curves have proven to be reliable.

Another important result of our model is related to the introduction of the stochastic component through a peculiar type of Poisson approximation that is computationally very efficient. Stochasticity is usually modelled as a Markov process [49] and simulated using the Gillespie algorithm [48], which can become very slow when the population is divided in many groups [50]. Our results show that our simple approach is sensibly faster and predicts fairly similar epidemic curves.

The limitation of our Poisson approximation is related to the overestimation of the probability of spontaneous extinction. This could probably be easily corrected by using the Poisson approximation only for the number of new cases and not for the number of infected individuals. However, the main interest in modelling pandemic spread lies in predicting expected features of the epidemic curve and in evaluating control measures if an epidemic starts, not in predicting the probability for an epidemic to start.

Our stochastic simulations of an influenza pandemic show (see Table 3) that the length of the initial phase can vary significantly,

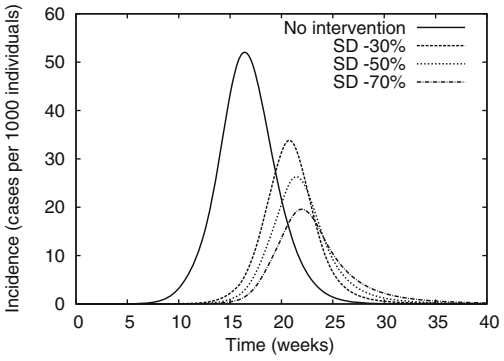

(a) Varying efficacy of social distancing measures

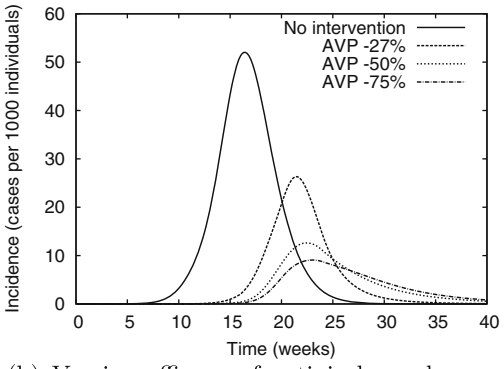

(b) Varying efficacy of antiviral prophylaxis

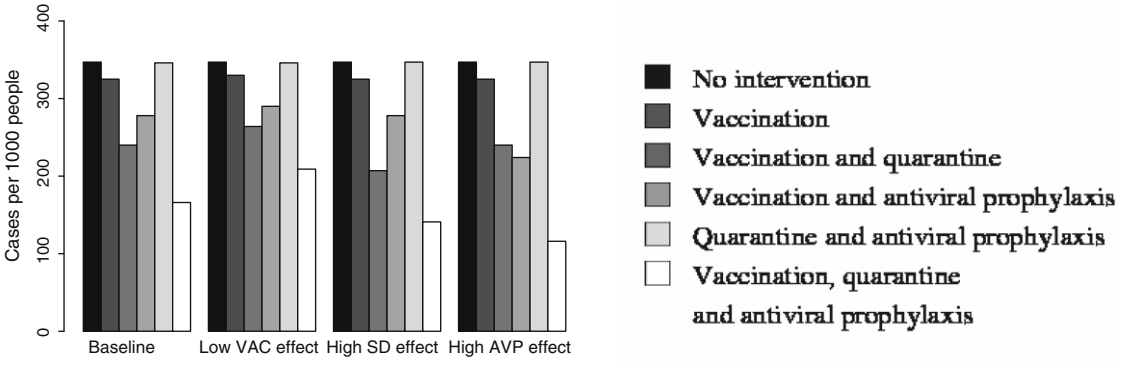

(c) Global attack rates for different scenarios and intervention efficacy

Fig. 8. Predicted effectiveness of combined control measures under different assumptions on the efficacy of vaccination, social distancing measures and antiviral prophylaxis. The baseline is $R_0 = 1.8$, $AR = 35\%$, social distancing (SD) measures reducing community transmission by 50%, vaccination (VAC) 70% effective, and antiviral prophylaxis (AVP) reducing household transmission by 27%. (a) epidemic dynamics without intervention (solid line) and for different levels of SD: 30% (dashed line), 50% (dotted line) or 70% (dashed-dotted line) effective. (b) Epidemic dynamics without intervention (solid line) and for different levels of AVP: 27% (dashed line), 50% (dotted line) or 75% (dashed-dotted line) effective. (c) Total attack rates (cases per 1000 people) for different intervention scenarios and intervention efficacy. Panel 1 (baseline): VAC 70%, SD 50%, AVP 27%. Panel 2 (low vaccination efficacy): VAC 50%, SD 50%, AVP 27%. Panel 3 (strong reduction in community contacts): VAC 70%, SD 70%, AVP 27%. Panel 4 (quick identification and prophylaxis of cases): VAC 70%, SD 50%, AVP 50%.

as the overall shape of the epidemic curve (i.e. in the incidence at the peak, that is more than 5% lower than in deterministic simulations). This variability can play an important role in the simulation of pandemic scenarios, and especially in the evaluation of possible control measures.

On the other hand, the initial variability in epidemic take off would be better assessed and probably less relevant if the national model was embedded in a model of worldwide pandemic spread, including infected individuals entering the country daily from abroad and enhancing the diffusion of the virus during the initial phase.

Embedding the model within a model of worldwide spread could also help in evaluating the time lag between the identification of the first cases in the world, the preparation of a pandemic vaccine (that would presumably start right afterward [51]) and the introduction of the virus in Italy. All these elements are crucial for the effectiveness of vaccination [27].

An important aspect of the model is the spatial structure, based on the Italian geography. The difference between the results obtained with and without spatial structure are clearly due to the way in which the 20 regions are connected when the spatial structure is included. Without spatial structure all individuals may have a contact with every other individual, while, when the spatial structure is included, contacts with individuals of a different region (and not always all of them) are possible only between adults of the more active subgroups. This slows significantly the initial spread of the infection (see Fig. 3), has a minor effect on the peak incidence (about 5% lower with spatial structure) and increases slightly the length of the epidemic.

The observed difference in epidemic timing may influence the evaluation of the effectiveness of possible control measures, as already noted. A correct assessment of the spatial transmission of the infection is thus essential. Although it is clear that transmission is more likely between individuals living in the same area, the weights to be given to contacts at different distances can be obtained only through accurate analysis of data on the spread of similar infections, such as seasonal influenza. Moreover, the choice of the optimal spatial structure in a patch model like ours could be controversial: we have chosen the regional scale mainly because of data availability, but Italian regions are very inhomogeneous as for surface and population and may not reflect adequately movements of individuals. Ciofi degli Atti et al. [19] chose a more detailed structure, based on the 8101 municipalities, that are reasonably homogeneous in surface, but extremely heterogeneous in population (between few dozens and millions of individuals). Such a scale would require many more data (or assumptions) on contact patterns and a more relevant computational time, especially in the stochastic version. Other groupings may reproduce better actual contacts and infection spread; a systematic comparison of models at different spatial scales could be helpful.

Depending on the parameter values, the simulated pandemic scenarios can be rather different. From the point of view of evalu-

ating interventions, the analysis show that a prompt intervention would help to reduce the epidemic intensity, although the actual impact of control measures would strongly depend on reproductive ratio R_0 of the infection (see Fig. 7) and on the efficacy of each control measure (Fig. 8a and b). In general, the combination of different control measures, if accurately planned, has synergistic effects and results in a sizable mitigation of the pandemic (Fig. 8c) even in the most pessimistic scenario considered here.

References

[1] K.S. Li, Y. Guan, J. Wang, G.J.D. Smith, K.M. Xu, L. Duan, A.P. Rahardjo, P. Puthavathana, C. Buranathai, T.D. Nguyen, A.T.S. Estoepangestie, A. Chaisingh, P. Auewarakul, H.T. Long, N.T.H. Hanh, R.J. Webby, L.L.M. Poon, H. Chen, K.F. Shortridge, K.Y. Yuen, R.G. Webster, J.S.M. Peiris, Genesis of a highly pathogenic and potentially pandemic H5N1 influenza virus in eastern Asia, Nature 430 (6996) (2004) 209.

[2] World Health Organization, Outbreak news, Avian influenza, Turkey-update, Weekly Epidemiological Record 81, 2006.

[3] World Health Organization, Epidemiology of WHO-confirmed human cases of avian A(H5N1) infection, Weekly Epidemiological Record, vol. 81, 2006.

[4] A.S. Monto, Vaccines and antiviral drugs in pandemic preparedness, Emerg. Infect. Dis. 12 (2006) 55.

[5] I. Stephenson, I. Gust, M.P. Kieny, Y. Pervikov, Development and evaluation of influenza pandemic vaccines, Lancet Infect. Dis. 6 (2006) 71.

[6] Influenza team (ECDC), Pandemic preparedness in the European Union – multi-sectoral planning needed, Eurosurveillance 12 (2007).

[7] World Health Organization, WHO global influenza preparedness plan: the role of WHO and recommendations for national measures before and during pandemics, 2005.

[8] R.J. Glass, L.M. Glass, W.E. Beyeler, H.J. Min, Targeted social distancing design for pandemic influenza, Emerg. Infect. Dis. 12 (2006) 1671.

[9] B.C. Chun, Modelling the impact of pandemic influenza, J. Prev. Med. Public Health 38 (2005) 379.

[10] A. Doyle, I. Bonmarin, D. Levy-Bruhl, Y.L. Le Strat, J.C. Desenclos, Influenza pandemic preparedness in France: modelling the impact of interventions, J. Epidemiol. Commun. Health 60 (5) (2006) 399.

[11] EPICO working group, Modelling scenarios of diffusion and control of pandemic influenza, Italy, Eurosurveillance 12(1) (2007) 3105.

[12] N.M. Ferguson, D.A.T. Cummings, C. Fraser, J.C. Cajka, P.C. Cooley, D.S. Burke, Strategies for mitigating an influenza pandemic, PNAS 103 (2006) 5935.

[13] T. Germann, K. Kadau, I.M. Longini, C.A. Macken, Mitigation strategies for pandemic influenza in the United States, PNAS 103 (2006) 5935.

[14] E. Hak, M.J. Meijboom, E. Buskens, Modelling the health–economic impact of the next influenza pandemic in the Netherlands, Vaccine 24 (2006) 6756.

[15] I.M. Longini, M.E. Halloran, A. Nizam, Y. Yang, Containing pandemic influenza with antiviral agents, Am. J. Epidemiol. 159 (2004) 623.

[16] I.M. Longini, A. Nizam, S. Xu, K. Ungchusak, W. Hanshaoworakul, D.A.T. Cummings, M.E. Halloran, Containing pandemic influenza at the source, Science 309 (2005) 1083.

[17] R. Patel, I.M. Longini, M.E. Halloran, Finding optimal vaccination strategies for pandemic influenza using genetic algorithms, J. Theor. Biol. 234 (2005) 201.

[18] J.T. Wu, S. Riley, C. Fraser, G.M. Leung, Reducing the impact of the next influenza pandemic using household-based public health interventions, PLoS Med. 3 (2006) 1532.

[19] M.L. Ciofi degli Atti, S. Merler, C. Rizzo, M. Ajelli, M. Massari, P. Manfredi, C. Furlanello, G. Scalia Tomba, M. Iannelli, Mitigation measures for pandemic influenza in Italy: an individual based model considering different scenariosinfluenza, PLoS ONE 3 (3) (2008) e1790.

[20] J. Arino, F. Brauer, P. van den Driessche, J. Watmough, J.R. Wu, Simple models for containment of a pandemic, J. Roy. Soc. Interface 3 (2006) 453.

[21] R. Gani, H. Hughes, D. Fleming, T. Griffin, J. Medlock, S. Leach, Potential impact of antiviral drug use during influenza pandemic, Emerg. Infect. Dis. 11 (9) (2005) 1355.

[22] M.G. Roberts, M. Baker, L.C. Jennings, G. Sertsou, N. Wilson, A model for the spread and control of pandemic influenza in an isolated geographical region, J. Roy. Soc. Interface 4 (2007) 325.

[23] A. Flahault, E. Vergu, L. Coudeville, R.F. Grais, Strategies for containing a global influenza pandemic, Vaccine 24 (2006) 6751.

[24] R.F. Grais, J.H. Ellis, G.E. Glass, Assessing the impact of airline travel on the geographic spread of pandemic influenza, Eur. J. Epidemiol. 18 (2003) 1065.

[25] V. Colizza, A. Barrat, M. Barthelemy, A. Valleron, A. Vespignani, Modeling the worldwide spread of pandemic influenza: baseline case and containment interventions, PLoS Med. 4 (2007) 95.

[26] B.S. Cooper, R.J. Pitman, W.J. Edmunds, N.J. Gay, Delaying the international spread of pandemic influenza, PLoS Med. 3 (2006) 845.

[27] C. Rizzo, A. Lunelli, A. Pugliese, A. Bella, P. Manfredi, G.P. Scalia Tomba, M. Iannelli, M.L. Ciofi degli Atti, Scenarios of diffusion and control of an influenza pandemic in Italy, Epidemiol. Infect. 136 (2008) 1650.

[28] D.M. Fleming, A.J. Elliot, Lessons from 40 years' surveillance of influenza in England and Wales, Epidemiol. Infect. 136 (2008) 866.

[29] Ministero della Salute, Piano nazionale di preparazione e risposta ad una pandemia influenzale. <http://www.ministerosalute.it/imgs/C_17_pubblicazioni_511_allegato.pdf>, 2006.

[30] N.M. Ferguson, D.A.T. Cummings, S. Cauchemez, C. Fraser, S. Riley, A. Meeyai, S. Iamsirithaworn, D.S. Burke, Strategies for containing an emerging influenza pandemic in Southeast Asia, Nature 437 (2005) 209.

[31] S. Cauchemez, F. Carrat, C. Viboud, A.J. Valleron, P.Y. Boelle, A Bayesian MCMC approach to study transmission of influenza: application to household longitudinal data, Stat. Med. 23 (2004) 3469.

[32] J.M. Hyman, T. LaForce, Bioterrorism: mathematical modeling applications in Homeland security, Frontiers in Applied Mathematics, SIAM, 2003, pp. 215–240 (Chapter 10).

[33] R.M. Anderson, R.M. May, Infectious Diseases of Humans: Dynamics and Control, Oxford University, Oxford, 1991.

[34] P. Manfredi, J.R. Williams, Realistic population dynamics in epidemiological models: the impact of population decline on the dynamics of childhood infectious diseases. Measles as an example, Math. Biosci. 192 (2004) 153.

[35] J. Mossong, N. Hens, M. Jit, P. Beutels, K. Auranen, R. Mikolajczyk, M. Massari, S. Salmaso, G. Scalia Tomba, J. Wallinga, J. Heijne, M. Sadkowska-Todys, M. Rosinska, W.J. Edmunds, Social contacts and mixing patterns relevant to the spread of infectious diseases, PLoS Med. 5 (2008) 381.

[36] O. Diekmann, J. Heesterbeek, Mathematical Epidemiology of Infectious Diseases, Chichester, Wiley, New York, 2000.

[37] O. Diekmann, J.A.P. Heesterbeek, J.A.J. Metz, On the definition and the computation of the basic reproduction ratio R0 in models for infectious diseases in heterogeneous populations, J. Math. Biol. 28 (1990) 365.

[38] G. Chowell, C.E. Ammon, N.W. Hengartner, J.M. Hyman, Transmission dynamics of the great influenza pandemic of 1918 in Geneva, Switzerland: assessing the effects of hypothetical interventions, J. Theor. Biol. 241 (2006) 193.

[39] G. Chowell, H. Nishiura, L.M. Bettencourt, Comparative estimation of the reproduction number for pandemic influenza from daily case notification data, J. Roy. Soc. Interface 4 (2007) 155.

[40] I.M. Longini, A mathematical model for predicting the geographic spread of new infectious agents, Math. Biosci. 90 (1987) 367.

[41] C.E. Mills, J.M. Robins, M. Lipsitch, Transmissibility of 1918 pandemic influenza, Nature 432 (2004) 904.

[42] L.A. Rvachev, I.M. Longini, A mathematical model for the global spread of influenza, Math. Biosci. 75 (1985) 3.

[43] J.P. Aparicio, H.G. Solari, Population dynamics: Poisson approximation and its relation to the Langevin process, Phys. Rev. Lett. 86 (2001) 4183.

[44] L. Gustafsson, Poisson simulation – a method for generating stochastic variations in continuous system simulation, Simulation 74 (5) (2000) 264.

[45] L. Gustafsson, M. Sternad, Bringing consistency to simulation of population models – Poisson simulation as a bridge between micro and macro simulation, Math. Biosci. 209 (2007) 361.

[46] H.G. Solari, M.A. Natiello, Stochastic population dynamics: the Poisson approximation, Phys. Rev. E 67 (2003) 031918.

[47] M. Nuño, T.A. Reichert, G. Chowell, A.B. Gumel, Protecting residential care facilities from pandemic influenza, Proc. Natl. Acad. Sci. 105 (30) (2008) 10625.

[48] D.T. Gillespie, Exact stochastic simulation of coupled chemical reactions, J. Phys. Chem. 81 (25) (1977) 2340.

[49] H. Andersson, T. Britton, Stochastic Epidemic Models and Their Statistical Analysis, Springer, 2000.

[50] F. Débarre, S. Bonhoeffer, R.R. Regoes, The effect of population structure on the emergence of drug resistance during influenza pandemics, J. Roy. Soc. Interface 4 (16) (2007) 893.

[51] R. Daems, G. Del Giudice, R. Rappuoli, Anticipating crisis: towards a pandemic flu vaccination strategy through alignment of public health and industrial policy, Vaccine 23 (2005) 5732.